

# Tribo- and Tribocorrosion Properties of Magnesium AZ31 Alloy

Alexandre Mégret <sup>1,2</sup>, Loïc Prince <sup>1,2</sup>, Marie-Georges Olivier <sup>2</sup> and Véronique Vitry <sup>1,\*</sup>

<sup>1</sup> Metallurgy Department, University of Mons, 20 Place du Parc, 7000 Mons, Belgium

<sup>2</sup> Materials Science Department, University of Mons, 20 Place du Parc, 7000 Mons, Belgium

\* Correspondence: veronique.vitry@umons.ac.be

**Abstract:** In automotive and aerospace fields, the use of lightweight materials is required. Magnesium and its alloys combine a low density with high mechanical properties and excellent thermal conductivity. However, those materials suffer from low corrosion and wear resistances. The combined action of corrosion and wear is also critical for these materials. Tribocorrosion of magnesium alloy AZ31 has been investigated with reciprocal sliding wear as a function of the applied load in dry and wet (NaCl) conditions. The study shows that the main wear mechanisms were adhesion, abrasion, and oxidation in dry sliding wear while no adhesion was found in wet sliding wear. Corrosion of the worn surface occurs also in wet sliding wear. It is interesting to notice that wear is less pronounced in wet sliding wear than in dry sliding wear due to the natural lubrication of the NaCl electrolyte. Only severe conditions, high normal load, and wet conditions bring magnesium AZ31 alloy in filiform corrosion.

**Keywords:** magnesium AZ31; reciprocal sliding wear; corrosion; coefficient of friction

## 1. Introduction

The automotive, electronics, and aerospace sectors, which call for the use of lightweight materials, are drawn to magnesium and its alloys because of their combination of lightness and high mechanical properties [1,2]. Magnesium has a density of 1740 kg/m<sup>3</sup> and a Young's modulus of 44 GPa. The characteristics of these alloys are their excellent thermal conductivity, electromagnetic damping resistance, biocompatibility, machinability, and recyclable nature [3]. Applications with severe weight restrictions, such as aircraft and automotive components, have given magnesium (Mg) alloys a lot of attention [4,5]. The primary issues with these metals are their extremely poor corrosion and wear resistances. The literature attributes the behaviour to the strong chemical activity of magnesium as well as to the unstable, imperfect natural oxide layer that coats its surface [6,7]. Understanding not just the wear and corrosion properties but also the tribocorrosion properties of magnesium is essential given the potential of the magnesium alloys. As a result of interaction between wear and corrosion synergy, materials degrade more quickly than if wear or corrosion occurred individually [8]. One of the distinctive electrochemical test methods is the tribo-electrochemical approach, which uses a tribometer combined with a potentiostat to detect electrochemical reactions of the surface that is being mechanically abraded [9]. The scratched electrode method, which creates a bare surface by removing the passive coating from the tested materials, is comparable to this method in that it analyses the associated electrochemical response, such as transient current and transient potential [10]. The electrochemical reactions help to better understand the dissolution of metal on film free areas, the reconstruction of oxide/hydroxide layers, and the recovery of surface films by providing information on the healing process taking place on the scratched surface. Thus, the mechanical investigation of the corrosion behaviour of various passive metallic materials is carried out using the scratched electrode technique and the tribo-electrochemical approach [11]. Recently, the scratched electrode method has been used to study the corrosion of pure Mg and Mg-Li alloys [12,13]. However, published works on the wear behaviour of AZ31 alloy are limited in reciprocating sliding mode despite the technological importance of the



**Citation:** Mégret, A.; Prince, L.; Olivier, M.-G.; Vitry, V. Tribo- and Tribocorrosion Properties of Magnesium AZ31 Alloy. *Coatings* **2023**, *13*, 448. <https://doi.org/10.3390/coatings13020448>

Academic Editor: Esmail Sadeghi

Received: 10 December 2022

Revised: 2 February 2023

Accepted: 8 February 2023

Published: 16 February 2023



**Copyright:** © 2023 by the authors. Licensee MDPI, Basel, Switzerland. This article is an open access article distributed under the terms and conditions of the Creative Commons Attribution (CC BY) license (<https://creativecommons.org/licenses/by/4.0/>).

alloy [14]. Most of the published works use the pin-on-disc method or characterize other magnesium alloys. The comparison between dry and wet sliding wear under the same conditions for that alloy is also missing in the literature.

Unfortunately, the low corrosion and wear resistances of magnesium alloys prevent them from being used for a wide range of applications and increase the expenses for their maintenance [3,15,16]. Studying the simultaneous influence of wear and corrosion is thus of great importance for a development of magnesium in the industry. Thus, in this work, tribological and tribocorrosion measurements were performed on the AZ31 alloy in a 0.05 M NaCl solution. The intrinsic surface film of AZ31 was intentionally damaged using a tribometer. The influence of the load was studied by tribology and tribocorrosion. The morphology of the wear tracks and the wear mechanisms were studied and the abraded volumes were calculated. The electrolyte was analysed to quantify the amount of Mg in the solution. The corrosion and repassivation behaviour of the Mg scratched surface in the dilute NaCl solution was discussed.

## 2. Materials and Methods

The AZ31 magnesium alloy has been studied. AZ31 magnesium alloy sheets were supplied by KG Fridman AB (Karlstadt, Sweden) with the following composition: 2.5–3.5 wt.% Al, 0.7–1.3 wt.% Zn, 0.2 wt.% Mn, 0.05 wt.% Si, 0.05 wt.% Cu, 0.04 wt.% Ca, 0.005 wt.% Fe, 0.1 wt.% Ni, and Mg rest (Re = 160 MPa, Rm = 240 MPa, Vickers microhardness 60  $hv_{100}$ ). The samples have been chemically pickled in nitric acid and rinsed in deionized water and air before testing. [7]

The substrates have been characterized in terms of roughness, structure, and microstructure. Their roughness has been determined by a Zeiss 119 Surfcom 1400D-3DF apparatus (Oberkochen, Germany). The different roughness values have been measured (average roughness  $R_a$ , peak roughness  $R_p$ , and valley roughness  $R_v$ ). The average of five measurements has been taken. X-ray diffraction has been used to assess the phase constitution of the substrate (Bruker D5000 X-ray diffractometer, Billerica, MA, USA). The diffractometer is in  $\theta$ - $2\theta$  configuration with a cobalt anti-cathode ( $\lambda = 1.79 \text{ \AA}$ ).

The tribology measurements have been achieved with a Bruker TriboLab reciprocal tribometer in reciprocal wear configuration [17] equipped with an alumina counter body. The alumina ball is 4.8 mm in diameter. The test conditions have been defined to be the same in dry and wet sliding wear tests. 1  $\text{cm}^2$  of the sample has been immersed in NaCl 0.05 M. The normal load of analysis has been set to 2, 5, and 8 N for a test time of 30 min at room temperature. The sliding distance is determined by the frequency of the test (2 Hz) and the stroke length (2 mm). Friction coefficients of friction (COF), calculated by the ratio  $F_t/F_n$ , have been recorded at 0.1 s time intervals ( $F_t$  is the friction force and  $F_n$  is the normal force). During wet sliding wear tests, the open-circuit potential has been recorded with a Bio-Logic SP50 Potentiostat (Seyssinet-Pariset, France) in order to evaluate the tribocorrosion of the samples. A classical three-electrodes cell has been used, with the sample as working electrode, a Platinum wire as counter electrode, and an Ag/AgCl/KCl(sat) as reference electrode. The solutions have been analyzed after the tribotest by ICP-AES (Inductively Coupled Plasma-Atomic Emission Spectrometry) to evaluate their Mg content. The worn volumes have been calculated by the equation defined by Sharma et al. [18], making the assumption that the alumina ball does not wear. The morphology of the worn surfaces has been characterized with an Hirox 3D-digital microscope (Limonest, France) and a Hitachi SU8020 scanning electron microscope (Tokyo, Japan) and energy-dispersive X-ray spectroscopy (Thermo Fisher Scientific, Waltham, MA, USA).

## 3. Results

### 3.1. Substrate Characterizations

Figure 1 shows the XRD pattern of the AZ31 magnesium alloy substrate. The main phase constituting the substrate is  $\alpha$ -Mg (hexagonal phase). Intermetallic phases containing Al, Zn, and Mn cannot be observed in the XRD pattern due to the low amount in alloying

elements. The XRD characterization suggests a strong orientation of the  $\alpha$ -Mg phase in the (00c) and (10c) planes coming from the manufacturing process of magnesium sheets. Table 1 shows the roughness of the substrate: the average roughness is close to 1  $\mu\text{m}$ . The peak roughness is more important than the valley roughness, probably due to the presence of the intermetallic phases.

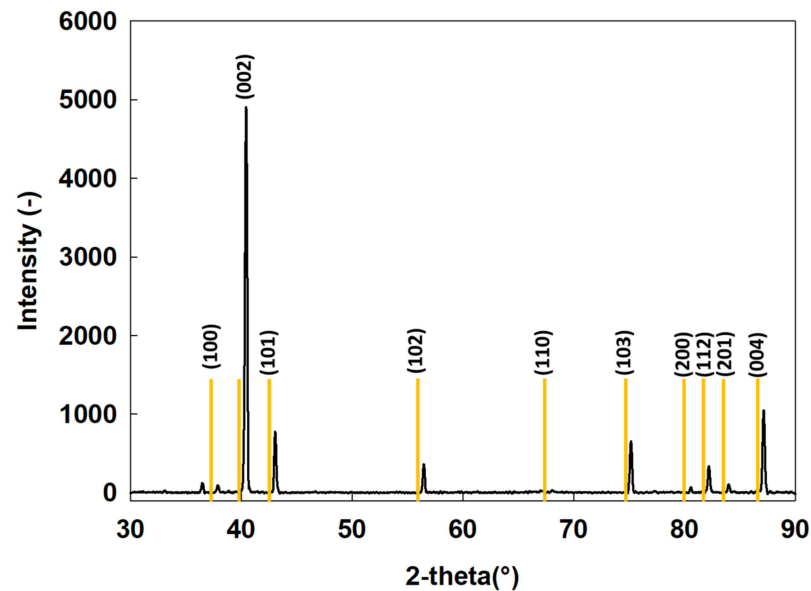


**Figure 1.** X-ray diffraction pattern of AZ31 magnesium alloy substrate.

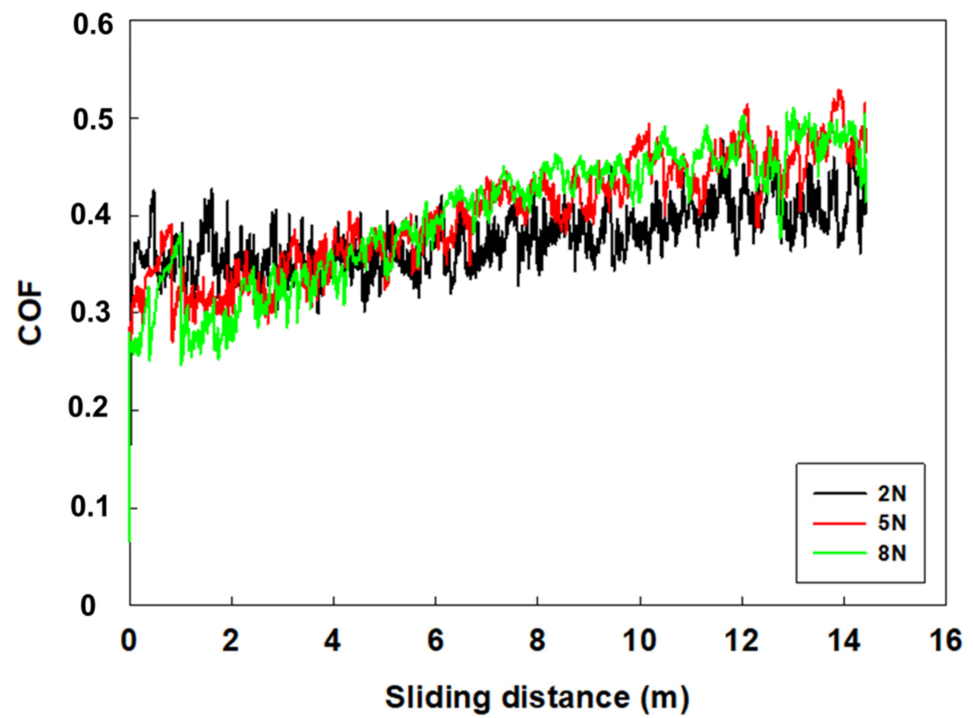
**Table 1.** Roughness characterization of AZ31 magnesium alloy substrate.

|                         |                             |
|-------------------------|-----------------------------|
| Average roughness $R_a$ | $0.96 \pm 0.09 \mu\text{m}$ |
| Peak roughness $R_p$    | $5.58 \pm 1.43 \mu\text{m}$ |
| Valley roughness $R_v$  | $2.52 \pm 0.68 \mu\text{m}$ |

### 3.2. Dry Sliding Wear (Tribology)

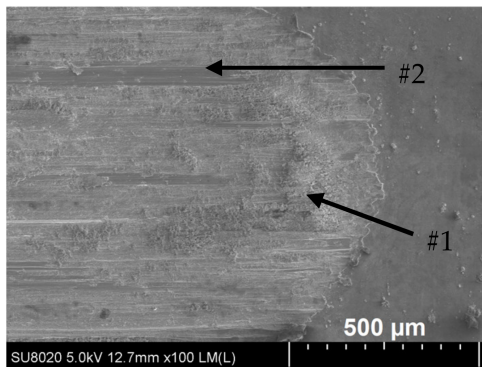
Worn surfaces, wear debris, and eventual wear of pin have been examined with the SEM-EDS. The wear mechanisms of AZ31 magnesium alloy have been characterized and compared with the usual wear mechanisms found in the literature: adhesion, abrasion, oxidation, delamination, plastic deformation, thermal softening, and melting [19–24].

Figure 2 gives the coefficient of friction of AZ31 samples as the function of the total sliding length. For all normal loads, COFs exhibit a similar behaviour [25,26]. With the increase of the sliding distance, COFs are increasing. When normal load is 2 N, the increase in COF is less pronounced than when the normal load is higher. Wear mechanisms are displayed in Figure 3. The main wear mechanism is abrasion, easily recognisable with the numbers of scratches that are present inside the wear track (areas noted #2 in the SEM-EDS of Figure 3). Those scratches or grooves, parallel to the sliding direction, are typical of the abrasion of harder particles (trapped between the alumina counter-body and the substrate). Those can come from intermetallic that are harder than Mg. EDS measurements shows that magnesium is the main element and that those areas contain a small oxygen content compared to the areas that noted #1. In these areas, oxidation is observed in the form of powder encrusted in the wear track. EDS analyses confirm the important presence of oxygen in the worn surface of AZ31 submitted to a higher normal load. The oxidation compound could be  $\text{Mg}(\text{OH})_2$  or  $\text{MgO}$ . Wear volumes are in the range of  $0.08 \text{ mm}^3$  for a load of 2 N to  $0.16 \text{ mm}^3$  for a load of 8 N for a total sliding distance of 15 m.



**Figure 2.** Coefficient of friction of AZ31 magnesium alloys as function of the applied normal load after dry sliding wear.

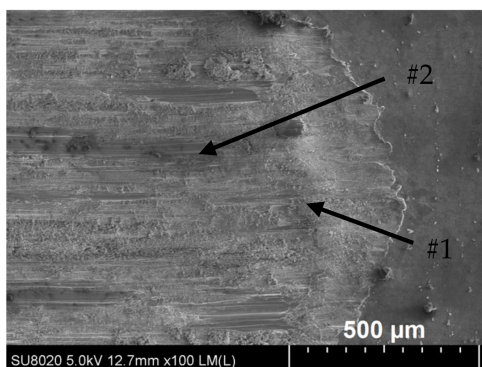
(a) SEM—2 N



(b) EDS—2 N

| wt.%           | O    | Mg   | Al  | Zn  |
|----------------|------|------|-----|-----|
| #1 (oxidation) | 32.7 | 63.0 | 1.7 | 0.8 |
| #2 (abrasion)  | 1.7  | 92.3 | 2.8 | 1.4 |

(c) SEM—5 N

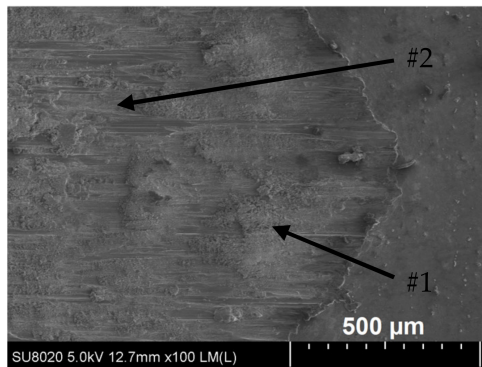


(d) EDS—5 N

| wt.%           | O    | Mg   | Al  | Zn  |
|----------------|------|------|-----|-----|
| #1 (oxidation) | 41.5 | 54.7 | 1.5 | 0.6 |
| #2 (abrasion)  | 2.0  | 91.8 | 2.5 | 2.2 |

**Figure 3.** Cont.

(e) SEM—8 N



(f) EDS—8 N

| wt.%           | O    | Mg   | Al  | Zn  |
|----------------|------|------|-----|-----|
| #1 (oxidation) | 40.8 | 54.5 | 1.7 | 1.4 |
| #2 (abrasion)  | 7.2  | 86.4 | 1.8 | 1.9 |

**Figure 3.** SEM and EDS analysis of AZ31 magnesium alloy in tribology: (a) SEM—2 N, (b) EDS—2 N, (c) SEM—5 N, (d) EDS—5 N, (e) SEM—8 N, (f) EDS—8 N.

The alumina counter body has also been analyzed by SEM-EDS and magnesium has been found on the  $\text{Al}_2\text{O}_3$  balls, meaning that adhesive wear is also present as a wear mechanism (Figure 4). The amount of Mg found on the ball is extremely low at 2 N and increases with the applied load. However, as alumina balls are much harder than AZ31 substrate, their wear can be neglected and the equation used to evaluate wear volumes can be validated.

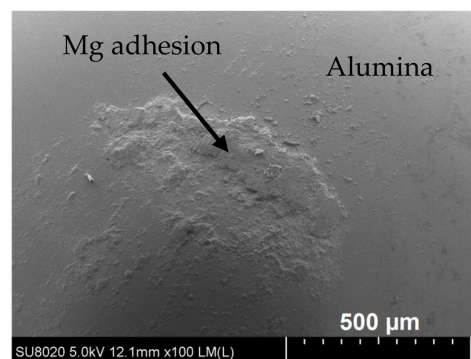


**Figure 4.** SEM picture of the alumina counter-body ball.

The debris have been analyzed and they contained between 70 and 90 wt.% in Mg, meaning that they are probably metallic magnesium particles eliminated from the worn track without extra oxidation. Plastic deformation, thermal softening, and melting have not been found since the applied normal loads are not sufficient to bring those wear mechanisms. Delamination, usually characterized by the formation of cracks perpendicular to the sliding direction and the detachment of sheet-like fragments, has not been observed in the chosen test conditions.

The influence of the normal load is not easily visible since COFs are comparable and the wear mechanisms are the same. Wear volume is however twice higher at 8 N than at 2 N, visible on the shape of the worn area. At low normal load, the worn area is long and thin while at high normal load, the worn area becomes shorter in length but wider. Oxidation is also more pronounced at a higher normal load in the wear track.

### 3.3. Wet Sliding Wear (Tribocorrosion)

The wear mechanisms are different in wet sliding wear compared to dry sliding wear. Indeed, the liquid medium participates in the removal of the debris from the wear track. Oxidation is also replaced by corrosion since the experiments are in a NaCl medium. Figure 5 shows the coefficient of friction during wet sliding wear of AZ31 magnesium alloy.

The COFs do not increase with the sliding distance, meaning that the liquid medium acts as a lubricant between the substrate and the alumina ball. The debris are also more easily evacuated and thus participate only a little in the wear mechanisms.

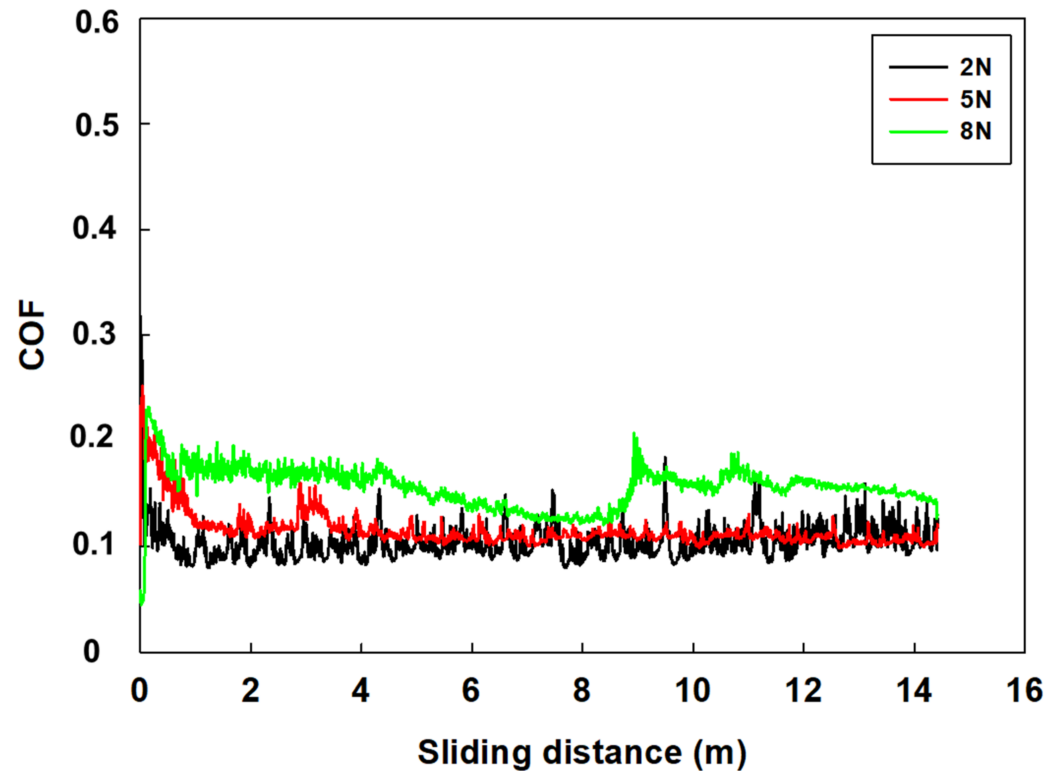
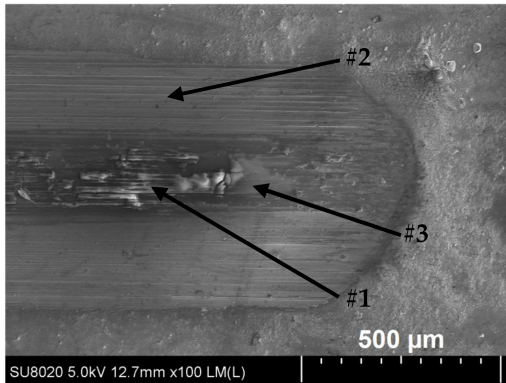


**Figure 5.** Coefficient of friction of AZ31 magnesium alloys as function of the applied normal load during wet sliding wear in 0.05 M NaCl.

Figure 6 displays the different SEM-EDS images of the wet sliding test (tribocorrosion) in an NaCl medium as a function of the applied normal load. Two different behaviours are found: at a low normal load, the traditional wear mechanisms are found while at a high normal load, filiform corrosion is observed on and around the wear track [27,28]. First, at 2 and 5 N, two main wear mechanisms are found: abrasion, recognizable by the parallel grooves to the sliding direction (areas #2) and corrosion (in the middle of the wear track, areas #1). The EDS characterizations clearly show that the amount of oxygen is less important in areas #2 than in areas #1. Chloride is found on the corroded parts. Some delamination of the oxide layer is also observed in the middle of the track, probably caused by harder asperities or harder intermetallic present on the substrate [8]. In these areas (#3), the oxygen content is lower than in the abrasion areas, meaning that they have been protected from high oxidation. Secondly, the substrates that have undergone the applied load of 8 N show filiform corrosion on their surface (area #1 of Figure 6e): these areas admit high oxygen and chloride contents of 45.1 wt.% and 2.7 wt.%, respectively. Inside the corrosion filaments, abrasion grooves are observed. A hypothesis for the formation of this corrosion is that as the applied load is high, local elastic deformations of the substrate lead to cracks in the passive layer of magnesium. With the chloride ions present in the liquid medium, filiform corrosion can be initiated, probably outside the wear track, and is able to diffuse inside the latter due to the removal of the protective layer.

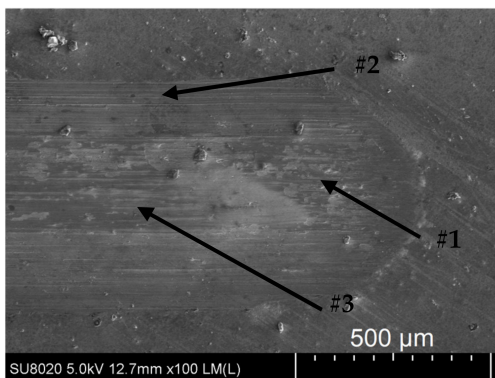
(a) SEM—2 N



(b) EDS—2 N

| wt.%              | O    | Mg   | Al  | Zn  | Cl  |
|-------------------|------|------|-----|-----|-----|
| #1 (corrosion)    | 17.1 | 73.3 | 2.8 | 1.3 | 0.5 |
| #2 (abrasion)     | 7.9  | 84.9 | 2.4 | 0.7 | -   |
| #3 (delamination) | 4.4  | 90.2 | 2.3 | 1.6 | -   |

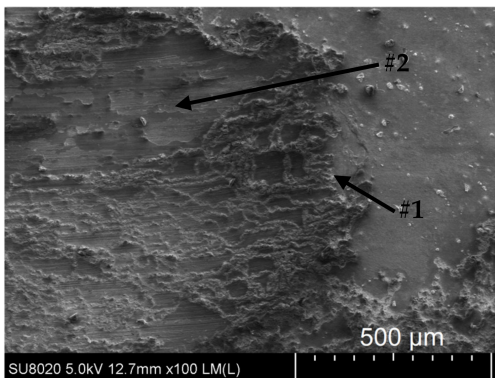
(c) SEM—5 N



(d) EDS—5 N

| wt.%              | O    | Mg   | Al  | Zn  | Cl  |
|-------------------|------|------|-----|-----|-----|
| #1 (corrosion)    | 33.4 | 57.4 | 1.8 | 1.1 | 0.4 |
| #2 (abrasion)     | 10.8 | 79.4 | 2.6 | 1.3 | -   |
| #3 (delamination) | 5.3  | 87.0 | 3.0 | 0.8 | -   |

(e) SEM—8 N



(f) EDS—8 N

| wt.%                    | O    | Mg   | Al  | Zn  | Cl  |
|-------------------------|------|------|-----|-----|-----|
| #1 (filiform corrosion) | 45.1 | 34.7 | 3.2 | 1.6 | 2.7 |
| #2 (abrasion)           | 20.7 | 68.9 | 2.9 | 1.5 | -   |

**Figure 6.** SEM and EDS analysis of AZ31 magnesium alloy in tribocorrosion: (a) SEM—2 N, (b) EDS—2 N, (c) SEM—5 N, (d) EDS—5 N, (e) SEM—8 N, (f) EDS—8 N.

The alumina counter-bodies have been analyzed with SEM-EDS but no trace of Mg adhesion has been found. The liquid used during the tribology test acts as lubricant and thus adhesion between alumina and Mg is not possible whatever the applied load.

Figure 7 gives the amount of magnesium found in the solution after the wet sliding wear test as a function of the applied normal load. The Mg content increases with the applied load, meaning that the worn volume is bigger. With low normal loads (2 and 5 N), the worn volumes are relatively low, respectively, 0.008 mm<sup>3</sup> and 0.012 mm<sup>3</sup>. With 8 N as the normal load, the worn volume is much higher and reaches 0.055 mm<sup>3</sup>, probably due to the formation of filiform corrosion.

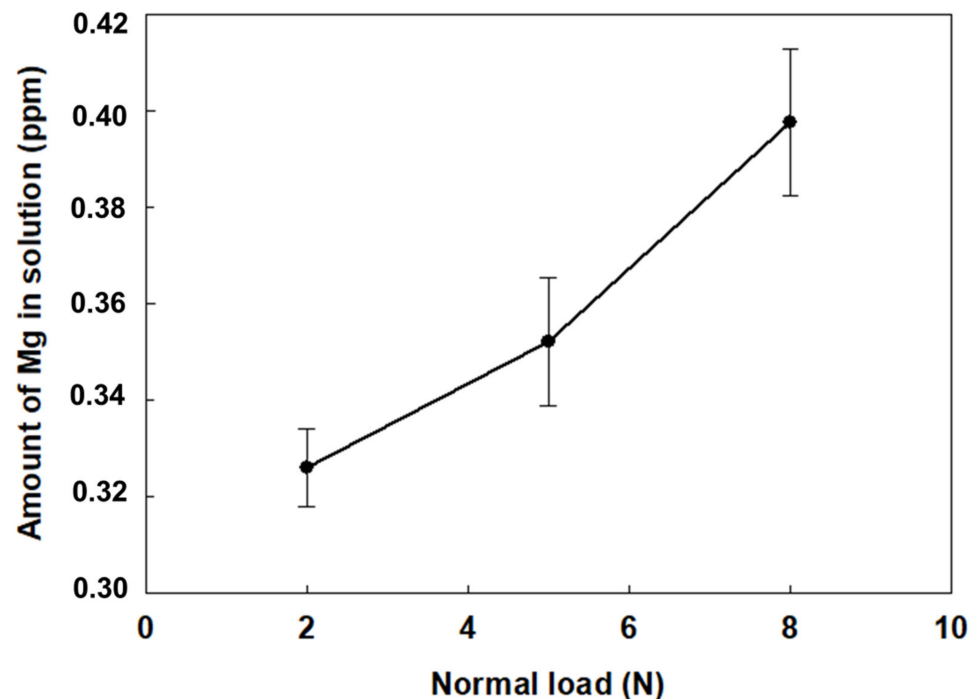


**Figure 7.** ICP-AES characterization of the solutions after wet sliding wear tests.

During wet sliding tests, the open-circuit potential has been recorded and is presented in Figure 8. For each normal load, OCP has been measured during 2 h: 30 min before the tribotest, 30 min during the tribotest and 1 h after the tribotest to evaluate the recovery of the OCP curve. Here again, the lowest normal loads show a homologous trend: OCP stabilizes after some minutes, then decreases when the tribotest starts (due to removal of the passivation layer of magnesium [1,5,29,30]). During the tribocorrosion test (30–60 min), OCP slightly increases (due to doping the system in energy). When the tribocorrosion test is finished and the ball is removed, OCP increases sharply (novel passivation of the substrate [1,5,29,30]) and could exceed the initial stabilized OCP before going to its stabilization value. At the highest normal load, the behaviour is totally different: the filiform corrosion created during the tribocorrosion test does not allow a sharp decrease of OCP; it decreased a little and fluctuated during the whole test. After the test, OCP increased before its stabilization.

In opposition to dry sliding behaviour, the highest normal load of wet sliding conditions differentiates from the two other loads: COFs are slightly higher and filiform corrosion has been found. Worn volumes are four to seven times higher than other normal load conditions. Wear mechanisms look the same for 2 and 5 N (corrosion and abrasion).

### 3.4. Comparison

Coefficients of friction do not show the same behaviour in dry or wet conditions. While in dry sliding wear, COFs increase continuously from 0.3 to 0.5 (the slope increases with the normal load) in wet sliding wear; COFs start around 0.2–0.3 and then decrease around 0.1 to 0.15. The wear volumes are thus higher in the case of dry sliding wear, from three to ten times higher than in wet sliding conditions. The use of a liquid acts as lubricant and permits the decrease in the coefficients of friction between the alumina counter-body and magnesium substrate. The debris are also more easily eliminated.

Results from the SEM show different wear mechanisms in dry and wet sliding wear. Although abrasion is observed in both cases, adhesion of magnesium on the counter alumina ball has been detected only in dry conditions. Oxidation and corrosion mechanisms appear, respectively, for dry and wet conditions. At high normal load (8 N), filiform corrosion is observed only in wet sliding wear.

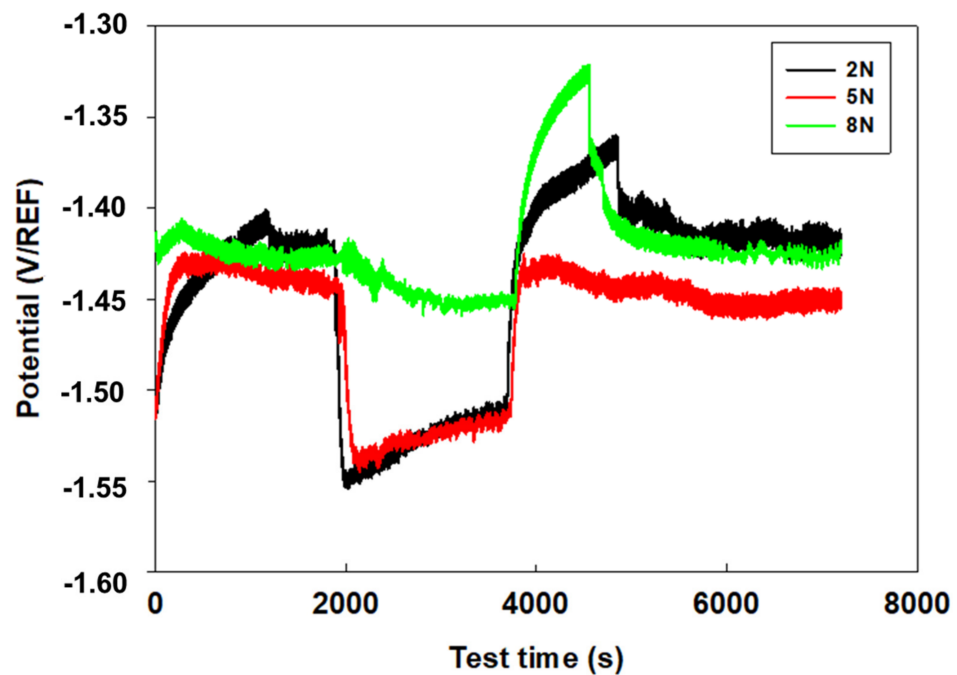


Figure 8. OCP recording during the wet sliding tests.

#### 4. Conclusions

A comparison between dry (tribology) and wet (tribocorrosion) sliding wear has been undertaken on a magnesium AZ31 alloy. An increase in the normal load has a low effect on dry sliding wear since the wear mechanisms remain the same (oxidation, abrasion, and adhesion). Only the wear volume shows an increase at higher normal loads, probably coming from higher oxidation in the wear track. Oppositely, the effect of normal load on wet sliding wear tests shows interesting features: although wear volumes are small (3–10 times lower than in tribology), the tendency to form filiform corrosion seems to be increased by higher normal loads. The reason could be a more difficult repassivation because more matter is abraded during the wear test. Wear mechanisms are different: adhesion and oxidation have not been observed but the latter has been replaced by corrosion. Abrasion is always observed and seems to be the major wear mechanism for the tested normal loads. Coefficients of friction are lower in the case of tribocorrosion due to the lubrication induced by the corrosion medium.

**Author Contributions:** Conceptualization, A.M., L.P., V.V.; methodology, A.M., L.P.; investigation, A.M., L.P.; resources, M.-G.O., V.V.; writing—original draft preparation, A.M., L.P.; writing—review and editing, M.-G.O., V.V.; funding acquisition, M.-G.O., V.V. All authors have read and agreed to the published version of the manuscript.

**Funding:** This research was funded under the ARC scheme—grant Sealcera.

**Institutional Review Board Statement:** Not applicable.

**Informed Consent Statement:** Not applicable.

**Data Availability Statement:** Not applicable.

**Acknowledgments:** They also would like to thank Materia Nova for SEM-EDS characterizations.

**Conflicts of Interest:** The authors declare no conflict of interest.

## References

1. Demirci, E.E.; Arslan, E.; Ezirmik, K.V.; Baran, Ö.; Totik, Y.; Efeoglu, I. Investigation of wear, corrosion and tribocorrosion properties of AZ91 Mg alloy coated by micro arc oxidation process in the different electrolyte solutions. *Thin Solid Film.* **2013**, *528*, 116–122. [[CrossRef](#)]
2. Prince, L.; Rousseau, M.A.; Noirfalise, X.; Dangreau, L.; Coelho, L.B.; Olivier, M.G. Inhibitive effect of sodium carbonate on corrosion of AZ31 magnesium alloy in NaCl solution. *Corros. Sci.* **2020**, *179*, 109131. [[CrossRef](#)]
3. Esmaily, M.; Svensson, J.E.; Fajardo, S.; Birbilis, N.; Frankel, G.S.; Virtanen, S.; Arrabal, R.; Thomas, S.; Johansson, L.G. Fundamentals and advances in magnesium alloy corrosion. *Prog. Mater. Sci.* **2017**, *89*, 92–193. [[CrossRef](#)]
4. Fernández-López, P.; Alves, S.A.; Azpitarte, I.; San-José, J.T.; Bayón, R. Corrosion and tribocorrosion protection of novel PEO coatings on a secondary cast Al-Si alloy: Influence of polishing and sol-gel sealing. *Corros. Sci.* **2022**, *207*, 110548. [[CrossRef](#)]
5. Liu, S.; Li, G.; Qi, Y.; Peng, Z.; Ye, Y.; Liang, J. Corrosion and tribocorrosion resistance of MAO-based composite coating on AZ31 magnesium alloy. *J. Magnes. Alloys* **2021**, *10*, 3406–3417. [[CrossRef](#)]
6. Pezzato, L.; Angelini, V.; Brunelli, K.; Martini, C.; Dabalà, M. Tribological and corrosion behavior of PEO coatings with graphite nanoparticles on AZ91 and AZ80 magnesium alloys. *Trans. Nonferrous Met. Soc. China* **2018**, *28*, 259–272. [[CrossRef](#)]
7. Prince, L.; Noirfalise, X.; Paint, Y.; Olivier, M. Corrosion mechanisms of AZ31 magnesium alloy: Importance of starting pH and its evolution. *Mater. Corros.* **2022**, *73*, 1615–1630. [[CrossRef](#)]
8. Siddaiah, A.; Mao, B.; Kasar, A.K.; Liao, Y.; Menezes, P.L. Influence of laser shock peening on the surface energy and tribocorrosion properties of an AZ31B Mg alloy. *Wear* **2020**, *462–463*, 203490. [[CrossRef](#)]
9. Azzi, M.; Szpunar, J.A. Tribo-electrochemical technique for studying tribocorrosion behavior of biomaterials. *Biomol. Eng.* **2007**, *24*, 443–446. [[CrossRef](#)]
10. Thangaraj, B.; Toshiyasu, N. Localized Electrochemical Impedance Spectroscopy Observation on Scratched Epoxy Coated Carbon Steel in Saturated Ca(OH)<sub>2</sub> with Various Chloride Concentration. *J. Anal. Bioanal. Tech.* **2016**, *7*, 2. [[CrossRef](#)]
11. Manhabosco, T.M.; Tamborim, S.M.; dos Santos, C.B.; Müller, I.L. Tribological, electrochemical and tribo-electrochemical characterization of bare and nitrided Ti6Al4V in simulated body fluid solution. *Corros. Sci.* **2011**, *53*, 1786–1793. [[CrossRef](#)]
12. Yan, Y.; Zhou, P.; Gharbi, O.; Zeng, Z.; Chen, X.; Volovitch, P.; Ogle, K.; Birbilis, N. Investigating ion release using inline ICP during in situ scratch testing of an Mg-Li(-Al-Y-Zr) alloy. *Electrochem. Commun.* **2019**, *99*, 46–50. [[CrossRef](#)]
13. Wang, L.; Snihirova, D.; Deng, M.; Vaghefinazari, B.; Höche, D.; Lamaka, S.V.; Zheludkevich, M.L. Revealing physical interpretation of time constants in electrochemical impedance spectra of Mg via Tribo-EIS measurements. *Electrochim. Acta* **2021**, *404*, 139582. [[CrossRef](#)]
14. Shen, M.; Zhu, X.; Han, B.; Ying, T.; Jia, J. Dry sliding wear behaviour of AZ31 magnesium alloy strengthened by nanoscale SiCp. *J. Mater. Res. Technol.* **2021**, *16*, 814–823. [[CrossRef](#)]
15. Lamaka, S.V.; Vaghefinazari, B.; Mei, D.; Petrauskas, R.P.; Höche, D.; Zheludkevich, M.L. Comprehensive screening of Mg corrosion inhibitors. *Corros. Sci.* **2017**, *128*, 224–240. [[CrossRef](#)]
16. Li, Q.; Lu, H.; Li, D.Y. Effect of recovery treatment on the wear resistance of surface hammered AZ31 Mg alloy. *Wear* **2019**, *426–427*, 981–988. [[CrossRef](#)]
17. Ayerdi, J.; Aginagalde, A.; Llavori, I.; Bonse, J.; Spaltmann, D.; Zabala, A. Ball-on-flat linear reciprocating tests: Critical assessment of wear volume determination methods and suggested improvements for ASTM D7755 standard. *Wear* **2021**, *470–471*, 203620. [[CrossRef](#)]
18. Sharma, S.; Sangal, S.; Mondal, K. On the optical microscopic method for the determination of ball-on-flat surface linearly reciprocating sliding wear volume. *Wear* **2013**, *300*, 82–89. [[CrossRef](#)]
19. Nguyen, Q.B.; Sim, Y.H.M.; Gupta, M.; Lim, C.Y.H. Tribology characteristics of magnesium alloy AZ31B and its composites. *Tribol. Int.* **2015**, *82*, 464–471. [[CrossRef](#)]
20. Taltavull, C.; Torres, B.; López, A.J.; Rams, J. Dry sliding wear behavior of AM60B magnesium alloy. *Wear* **2013**, *301*, 615–625. [[CrossRef](#)]
21. An, J.; Li, R.; Lu, Y.; Chen, C.M.; Xu, Y.; Chen, X.B.; Wang, L.M. Dry sliding wear behavior of magnesium alloys. *Wear* **2008**, *265*, 97–104. [[CrossRef](#)]
22. Aung, N.N.; Zhou, W.; Lim, L.E.N. Wear behaviour of AZ91D alloy at low sliding speeds. *Wear* **2008**, *265*, 780–786. [[CrossRef](#)]
23. Moheimani, S.K.; Keshtgar, A.; Khademzadeh, S.; Tayebi, M.; Rajaei, A.; Saboori, A. Tribological behaviour of AZ31 magnesium alloy reinforced by bimodal size B4C after precipitation hardening. *J. Magnes. Alloys* **2021**, *10*, 3267–3280. [[CrossRef](#)]
24. Liang, C.; Li, C.; Lv, X.X.; An, J. Correlation between friction-induced microstructural evolution, strain hardening in subsurface and tribological properties of AZ31 magnesium alloy. *Wear* **2014**, *312*, 29–39. [[CrossRef](#)]
25. Li, P.; Lei, M.K.; Zhu, X.P. Dry sliding tribological behavior of AZ31 magnesium alloy irradiated by high-intensity pulsed ion beam. *Appl. Surf. Sci.* **2010**, *257*, 72–81. [[CrossRef](#)]
26. Xia, S.; Liu, Y.; Fu, D.; Jin, B.; Lu, J. Effect of Surface Mechanical Attrition Treatment on Tribological Behavior of the AZ31 Alloy. *J. Mater. Sci. Technol.* **2016**, *32*, 1245–1252. [[CrossRef](#)]
27. Williams, G.; Grace, R. Chloride-induced filiform corrosion of organic-coated magnesium. *Electrochim. Acta* **2011**, *56*, 1894–1903. [[CrossRef](#)]
28. Williams, G.W.; Birbilis, N.; McMurray, H.N. Controlling factors in localised corrosion morphologies observed for magnesium immersed in chloride containing electrolyte. *Faraday Discuss.* **2015**, *180*, 313–330. [[CrossRef](#)]

29. Xu, L.; Liu, N.; Cao, L.; Wan, Y. Influences of electrolytes on tribocorrosion performance of MAO coating on AZ31B magnesium alloy in simulated body fluid. *Int. J. Appl. Ceram. Technol.* **2021**, *18*, 1657–1669. [[CrossRef](#)]
30. Pezzato, L.; Vranescu, D.; Sinico, M.; Gennari, C.; Settimi, A.G.; Pranovi, P.; Brunelli, K.; Dabalà, M. Tribocorrosion properties of PEO Coatings produced on AZ91 magnesium alloy with silicate- or phosphate-based electrolytes. *Coatings* **2018**, *8*, 202. [[CrossRef](#)]

**Disclaimer/Publisher’s Note:** The statements, opinions and data contained in all publications are solely those of the individual author(s) and contributor(s) and not of MDPI and/or the editor(s). MDPI and/or the editor(s) disclaim responsibility for any injury to people or property resulting from any ideas, methods, instructions or products referred to in the content.